Kinetically driven self assembly of highly ordered nanoparticle monolayers

TERRY P. BIGIONI[1], XIAO-MIN LIN[2], TOAN T. NGUYEN[1], ERIC I. CORWIN[1,3], THOMAS A. WITTEN[1,3] AND HEINRICH M. JAEGER[1,3]*

[1]James Franck Institute, University of Chicago, Chicago, Illinois 60637, USA
[2]Materials Science Division, Chemistry Division and Center for Nanoscale Materials, Argonne National Laboratory, Argonne, Illinois 60439, USA
[3]Department of Physics, University of Chicago, Chicago, Illinois 60637, USA
*e-mail: h-jaeger@uchicago.edu

Published online: 19 March 2006; doi:10.1038/nmat1611

When a drop of a colloidal solution of nanoparticles dries on a surface, it leaves behind coffee-stain-like rings of material with lace-like patterns or clumps of particles in the interior[1–6]. These non-uniform mass distributions are manifestations of far-from-equilibrium effects, such as fluid flows[1] and solvent fluctuations during late-stage drying[2]. However, recently a strikingly different drying regime promising highly uniform, long-range-ordered nanocrystal monolayers has been found[7,8]. Here we make direct, real-time and real-space observations of nanocrystal self-assembly to reveal the mechanism. We show how the morphology of drop-deposited nanoparticle films is controlled by evaporation kinetics and particle interactions with the liquid–air interface. In the presence of an attractive particle–interface interaction, rapid early-stage evaporation dynamically produces a two-dimensional solution of nanoparticles at the liquid–air interface, from which nanoparticle islands nucleate and grow. This self-assembly mechanism produces monolayers with exceptional long-range ordering that are compact over macroscopic areas, despite the far-from-equilibrium evaporation process. This new drop-drying regime is simple, robust and scalable, is insensitive to the substrate material and topography, and has a strong preference for forming monolayer films. As such, it stands out as an excellent candidate for the fabrication of technologically important ultra thin film materials for sensors, optical devices and magnetic storage media.

Figure 1a shows the extraordinary degree of monolayer perfection achievable with this technique, with ordering over areas covered by roughly 10^8 particles. The long-range ordering and compactness of the monolayer, the fact that there are no lace- or ring-like patterns, and the absence of any three-dimensional (3D) aggregates points to a mechanism substantially different from those reported previously for late-stage drying-mediated assembly[3–6,9], or for self assembly mediated by both the substrate–liquid and liquid–air interfaces[10]. Instead, the final results resemble those occurring when nanoparticles are contained at the interface of an immiscible fluid under equilibrium conditions[11–14].

We directly observed this monolayer self-assembly process under the highly non-equilibrium conditions of an evaporating drop. During evaporation, monolayer islands of Au nanocrystals appear on the top surface of the drop, plainly visible under an optical microscope, and grow as compact structures of uniform contrast (Fig. 2 and Supplementary Information, Movie). These islands eventually merge to form a continuous monolayer across the entire liquid–air interface (Fig. 1b). As the remaining liquid slowly evaporates, the contact line depins and recedes towards the centre of the substrate, laying the nanocrystal sheet down onto the substrate.

We found that both the evaporation kinetics and the amount of excess dodecanethiol ligand molecules affected monolayer formation at the liquid–air interface. If the evaporation rate was slowed significantly or the solutions were thoroughly cleaned of excess dodecanethiol, we observed no monolayer formation at the interface. Instead, we observed nanocrystals concentrating and depositing at the substrate edge[1], forming 3D crystals in the bulk[15], and depositing directly onto the substrate as a percolating monolayer on dewetting and drying[2] (see Supplementary Information, Fig. S1). These monolayers strongly resembled various structures reported earlier[1–6,9]. Adding a dodecanethiol volume fraction as small as 5×10^{-5} once again promoted kinetically induced monolayer growth at the liquid–air interface. Monolayers grown on the liquid–air interface consistently showed a high degree of ordering, and were compact over macroscopic dimensions.

These observations suggest that two key elements are required for the interfacial self-assembly mechanism: (i) rapid evaporation, to segregate particles near the liquid–air interface, and (ii) an attractive interaction between the particles and the liquid–air interface, to localize them on the interface. Together, this establishes a saturated 2D solution of particles on the liquid–air interface, from

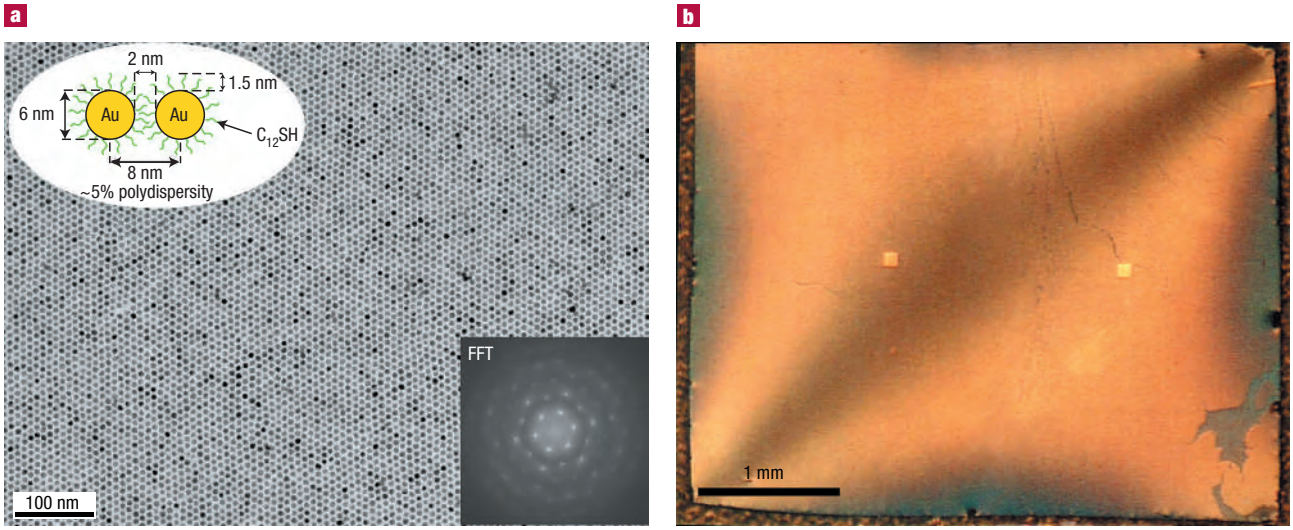

Figure 1 Gold nanocrystal monolayer. a, Micrograph of a typical monolayer produced by drop-casting 10 μl of a solution of dodecanethiol-ligated 6-nm gold nanocrystals onto a 3 mm × 4 mm substrate. The upper left inset schematically shows the arrangement of two neighbouring nanocrystals in the monolayer. The lower right inset is a fast Fourier transform of the image. **b**, Top view of a fully formed, compact nanocrystal monolayer on the top surface of a thin liquid droplet. The monolayer extends completely across the 3 mm × 4 mm Si_3N_4 substrate. The bright and dark patterns are due to light scattering from the curved surface of the pinned droplet. Mechanical damage in the bottom right corner and stress fractures in the upper right quadrant help visualize the monolayer. The two bright yellow squares are Si_3N_4 membrane TEM windows.

which 2D nucleation and growth can proceed. These ideas form the basis for a simple model of nanoparticle assembly that we can test against the measured domain growth rates.

For ordinary 2D growth, it is generally expected that the island areas will increase quadratically in time by nanoparticle diffusion and aggregation along the island perimeter. We find distinctly different growth laws, including linear and exponential behaviour. In the exponential regime, island growth follows either a strict exponential or a somewhat weaker, yet highly nonlinear growth law (Fig. 3a and b, respectively). In the linear regime, islands grow to a complete monolayer at a constant rate (Fig. 3c), with growth rates that vary from island to island. We also found that as long as island growth occurs on the liquid–air interface, a highly ordered monolayer results (Fig. 1a), irrespective of the growth law.

To understand the role of kinetics, we consider how particles from the bulk solution arrive on the top surface of the drop. Under ambient conditions, evaporation typically shrinks the centre thickness of the 3 mm × 4 mm drop by about 1 mm over 10 min; the remaining height is lost by advection. At the same time, nanocrystals diffuse a vertical distance $(2Dt)^{1/2} \sim 0.3$ mm, where the diffusion constant was estimated from the Stokes–Einstein relation $D = k_B T/6\pi\eta r \approx 73\ \mu m^2\ s^{-1}$. Here k_B is Boltzmann's constant, T the temperature, $\eta = 0.6$ cp the viscosity of toluene, and $r = 5$ nm the hydrodynamic radius of the nanocrystals. Therefore, the interface velocity is fast compared to diffusion, so the nanocrystals impinge on the descending interface as it moves towards the substrate.

In the reference frame of the interface, the evaporated solvent molecules must be replenished from the liquid phase below. Therefore, there must be a net relative flux of solvent molecules, and nanoparticles, towards the interface. In this case, nanocrystals will impinge on the interface with flux $f = -cv$, where c is the nanocrystal concentration and v is the velocity of the interface. A more detailed calculation using a height-dependent particle density in the diffusion equation gives the same result for the flux.

If there is a finite particle–interface interaction, nanocrystals hitting the interface move along the liquid surface for a time, τ, covering an interfacial diffusion length $\delta = (4D_{int}\tau)^{1/2}$. D_{int} is a diffusion constant for the liquid–air interface. If a nanocrystal impinges on the interface within a distance δ from an island it can, on average, diffuse to the island perimeter and be incorporated, otherwise it desorbs back into the bulk. Alternatively, a nanocrystal impinging directly on an island might be incorporated into its interior by diffusing across the island until it encounters either a defect or the perimeter. For simplicity we assume that, once incorporated, the particles do not leave the islands. In the limits $\delta \to 0$ and $f \to 0$, it becomes difficult to nucleate islands. To achieve nucleation, f must exceed a value f_o such that the critical surface density, $\rho_o = f_o\tau$, is reached. This predicts that a boundary should exist, given by $f_o = 4\rho_o D_{int}/\delta^2$, below which no monolayer growth occurs. The above assumptions make it possible to model monolayer growth kinetics on the liquid interface in a manner analogous to vacuum deposition of material onto a solid surface[16,17], despite the fact that nanoparticles dissolved in a viscous medium are subjected to flows.

The island growth laws that emerge from this model depend on the scaling of the collection areas with island size. For diffusion to the island perimeter, the collection area is a band of width δ surrounding each island from which nanocrystals successfully migrate to the island. The area of this band scales linearly with mean island radius R, as $A_{diff} = 2\pi R\delta + \pi\delta^2$. For direct incorporation, the collection area is simply the island area, $A = \pi R^2$. This leads to a net growth rate $dA/dt = k(A + A_{diff}) = k\pi(R + \delta)^2$, where $k = fa$ is the rate constant and a the area per particle. In the limit $\delta/R \ll 1$, exponential island growth emerges. Just after nucleation $\delta/R \gg 1$ and initial island growth will be linear; however, islands in this regime are generally still too small to be detected optically.

When $R + \delta$ approaches half of the island–island spacing, we can no longer consider islands in isolation because they compete with their neighbours to collect nanocrystals. Each island's

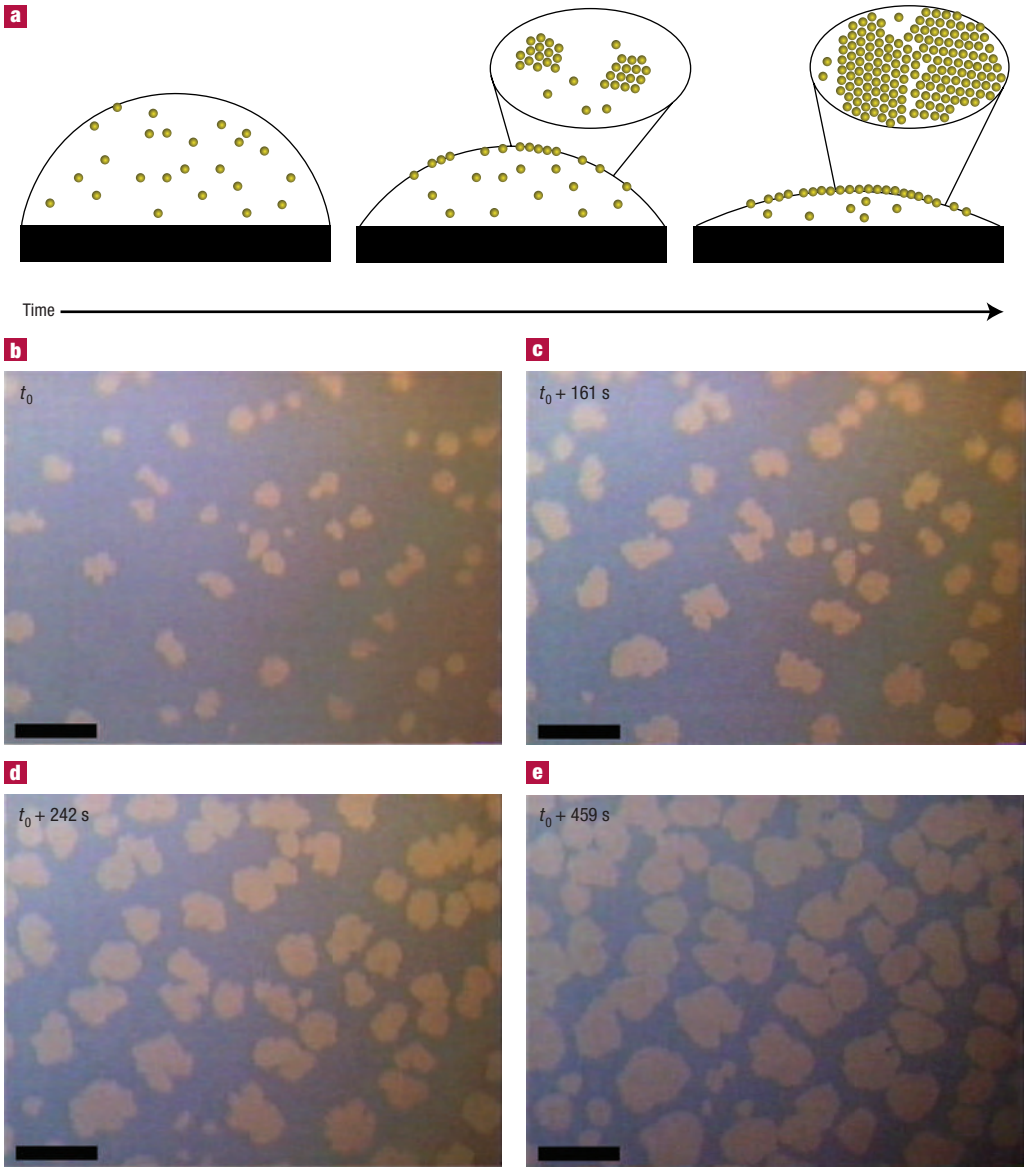

Figure 2 Monolayer island growth. a, Schematic diagram of the self-assembly process during the early stages of drying (not to scale), showing how nanocrystals are captured by a quickly receding liquid–air interface. **b–e**, Growth sequence of monolayer islands of 6-nm dodecanethiol-passivated gold nanocrystals as they appear under an optical microscope. Islands self-assemble on the top surface of an evaporating drop and appear light in colour. Scale bars are 50 μm. Illumination is from above.

collection area is, on average, limited to all points closer to it than any other island. This is its Voronoi cell (see Supplementary Information, Fig. S2), with area A_{vor} and effective radius R_{Vor}. The island growth rate is then determined only by the flux of nanocrystals into its cell. Thus, when $R + \delta > R_{Vor}$, $dA/dt = kA_{vor}$ and linear areal growth results.

Within this model, different growth regimes are entirely determined by the island size R and two parameters: the interfacial diffusion length (δ) and the flux of particles into the interface (f). Together, these capture the complex details of the evaporation conditions, solution composition and particle interactions. The resulting drop-casting phase diagram is shown in Fig. 4. This phase diagram delineates the expected signatures for interfacial island growth, as well as the boundary below which island growth at the liquid–air interface does not occur and particles are deposited directly onto the substrate.

A detailed examination of the observed growth regimes strongly supports this interfacial growth model. For linear island growth (Fig. 3c and the yellow areas in Fig. 4), the growth rate of each island is indeed proportional to its Voronoi cell area (Fig. 3c, inset). This clearly shows that the particle collection area consists of both A and A_{diff}, and that the diffusion timescales are much shorter than k^{-1}. From the largest Voronoi cells, we estimate a lower bound of ~25 μm for δ in this regime. The linear growth regime allows us to directly compare the observed monolayer growth rate with the flux predicted by the model. In Fig. 3c, the monolayer requires ~400 s to form, which corresponds to a flux of $f \sim 45\ \mu m^{-2}\ s^{-1}$. Fitting the model to the data gives a flux of $f = (51 \pm 7)\ \mu m^{-2}\ s^{-1}$ and a rate constant of $k = (2.8 \pm 0.4) \times 10^{-3}\ s^{-1}$, in good agreement with the direct growth time measurement. For the intermediate growth regime (blue areas in Fig. 4), we expect an intermediate δ. Indeed, fitting our model to the intermediate growth data shown in Fig. 3b

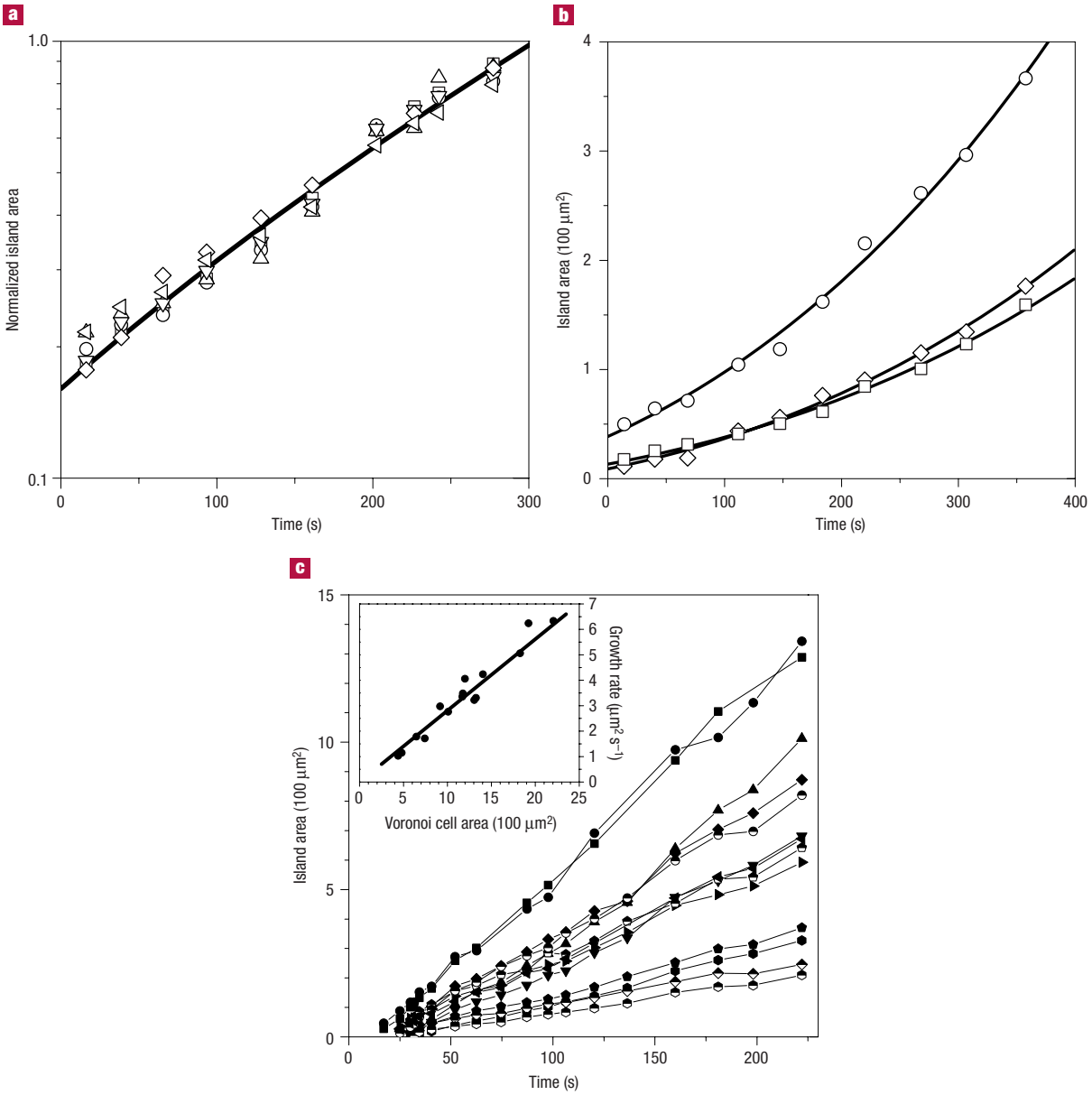

Figure 3 Island growth rates from individual islands tracked with video microscopy. Each panel represents a group of islands tracked over a single experiment. Three limits of growth are identified: exponential, intermediate and linear. **a**, Individual island areas from Fig. 2 increase roughly exponentially in time. Data were rescaled for best collapse. Fitting the growth model to the data gives $k = (4.0 \pm 1.0) \times 10^{-3}$ s^{-1} and $\delta = (0.08 \pm 0.06)$ μm. **b**, Individual island areas follow an intermediate growth law. Using $k = 1.6 \times 10^{-3}$ s^{-1} from the growth time, which corresponds to $f = 29$ μm^{-2} s^{-1}, fitting the model to the data gives $\delta = (5.1 \pm 0.3)$ μm. **c**, Thirteen individual islands, tracked over as much as two decades of area, show linear growth with widely differing growth rates. Inset: The average growth rate of each island is proportional to its average Voronoi cell area. Fitting the data gives a flux of $f = (51 \pm 7)$ μm^{-2} s^{-1} and a rate constant of $k = (2.8 \pm 0.4) \times 10^{-3}$ s^{-1}. This is in agreement with the monolayer growth time of ~400 s and the expected flux of $f \sim 45$ μm^{-2} s^{-1}. Particle concentrations were **a**, 3×10^{13} ml^{-1}, **b**, 3.4×10^{13} ml^{-1}, and **c**, 2.0×10^{13} ml^{-1}, and excess thiol volume fractions were **a**, ~5×10^{-5}, **b**, 1–2 $\times 10^{-4}$, and **c**, 6×10^{-4}.

gives $\delta \sim 5$ μm, such that δ/R is of order unity throughout the time window of the experiment. Finally, for the exponential growth regime (red areas in Fig. 4), we expect a small but finite δ. A fit of the full rate equation to the data in Fig. 3a gives $\delta \ll 1$ μm, so $\delta/R \ll 1$ and the collection area is approximately the island area throughout the observation time window. Using the experimental velocity $v \approx 1$ mm/26 min, single particle area $a = 55$ nm^2, and concentration $c \approx 3 \times 10^{13}$ ml^{-1}, we estimate $f \approx 20$ μm^{-2} s^{-1} and $k \approx 1.1 \times 10^{-3}$ s^{-1}. From the fit to the data in Fig. 3a, we obtain $f = (73 \pm 18)$ μm^{-2} s^{-1} and $k = (4.0 \pm 1.0) \times 10^{-3}$ s^{-1} suggesting, as $f = -cv$, that the particle concentration near the liquid–air interface is enhanced from the bulk value. This is consistent with small δ and v.

We can connect the measured diffusion lengths to a change in surface free energy on adsorption, $\Delta\sigma$. Considering a nanocrystal trapped at the liquid–air interface in a harmonic potential well of depth $U = \Delta\sigma a$, its residence time is $\tau = (1/\nu_o)\exp(U/k_B T)$. The attempt frequency ν_o can be estimated as the time for a

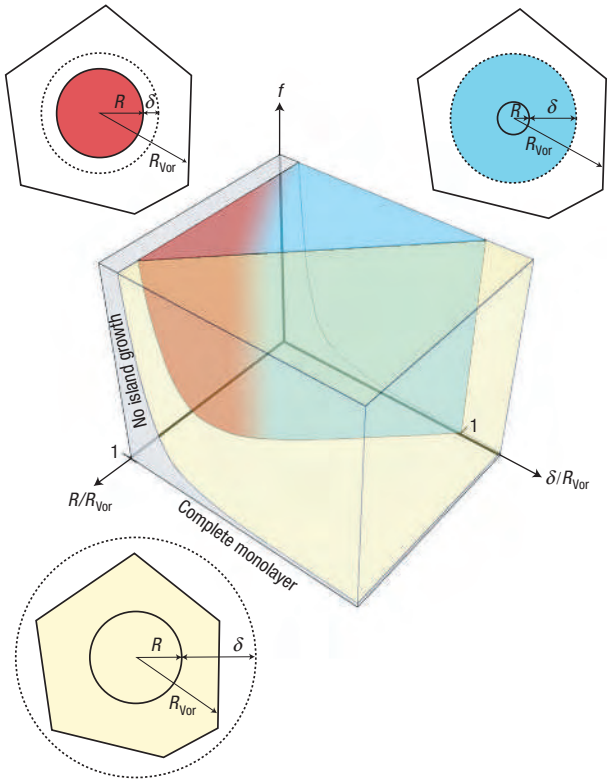

Figure 4 Phase diagram for drop casting. Experiments proceed in the R-direction, as the island radii grow in time. Island growth is governed by two parameters: the particle flux onto the liquid–air interface, f, and the distance particles diffuse along that interface, δ. Lengths are normalized by the Voronoi cell radius, R_{Vor}, which defines the maximal collection region. Island nucleation and growth occurs above the curved critical flux plane; no interfacial monolayer growth occurs below this boundary. Each growth rate is determined solely by the collection area. Linear growth occurs when $R+\delta > R_{Vor}$ (yellow region), because all particles that impinge on the interface can reach an island. Exponential growth occurs when $R+\delta < R_{Vor}$ and $\delta \ll R$ (red region). Intermediate growth occurs for larger δ (blue region). These three limiting cases are shown schematically, with the dominant collection area in colour. The solid circle depicts the island perimeter, the dotted circle represents the range of diffusion, and the polygon depicts the Voronoi cell.

nanocrystal to diffuse one diameter perpendicular to the interface, such that $v_o = 2D/(2r)^2$. Combining these relations, we have $\delta^2 = 8r^2 \exp(\Delta\sigma a/2k_B T)$, giving $\Delta\sigma \sim 0.35$ mN m^{-1} for $\delta = 0.08$ μm, $\Delta\sigma \sim 1.0$ mN m^{-1} for 5 μm, and $\Delta\sigma \sim 1.3$ mN m^{-1} for 25 μm. This shows that small changes in $\Delta\sigma$ can lead to large changes in δ, and that $\Delta\sigma$ can be amplified by the particle size to create a significant particle–interface interaction[11].

Experimentally, we found that solutions thoroughly cleaned of excess dodecanethiol, and solutions containing a low surface-tension solvent, show no island growth under ambient evaporation conditions. In other words, they remain below the critical nucleation boundary, consistent with $\delta \sim 0$. With the addition of excess dodecanethiol, the interfacial island nucleation and growth is greatly enhanced. Furthermore, for a solution with a small amount of excess thiol, it is even possible to cyclically change the evaporation rate to reversibly grow and dissolve islands on the interface. Although our experiments cannot elucidate the details of the underlying mechanism, this correlation suggests that the thiol concentration plays a key role in controlling the particle–interface interaction and the magnitude of δ. In general, δ might be tuned by particle size[11], surface tension[18] or osmotic pressure[19], which should lead to the realization of highly ordered monolayers of arbitrary materials in a wide range of experimental conditions.

Within this picture only two parameters, the particle flux f and the interfacial diffusion length δ, are required to capture the kinetics and energetics, and thereby the essential physics, of this drying-mediated assembly process. The drop-casting phase diagram shows that a sufficiently high flux, controlled by the evaporation rate and particle concentration, and a sufficiently large particle–interface interaction, parameterized by the interfacial diffusion length, are required to form 2D islands at the drop surface. This early stage island formation is a prerequisite for extended monolayers to form during the late stages of drying. If the flux is too small or the diffusion length is too short, stain- or lace-like particle aggregates are formed, characteristic of late-stage drying directly at the substrate interface.

This predicts that controlling the interaction between the particles and the liquid–air interface is the key to the realization of highly ordered monolayers. As these layers extend over macroscopic dimensions, there is no principal upper limit for the area to be covered.

METHODS

We formed the monolayers using a solution of monodisperse (<5%) dodecanethiol-ligated gold nanocrystals in toluene[7], with a typical size of 6 nm and particle concentration of roughly 2×10^{13} ml^{-1}. To this, we added a controlled amount of excess dodecanethiol, from 5×10^{-5} to 6×10^{-3} by volume. A 10 μl droplet of this solution, just sufficient to form a full monolayer, was deposited on a 3 mm × 4 mm substrate such that the contact line was pinned at the edges and the droplet was ~2 mm high. If higher concentrations are used, excess nanocrystals can deposit or nucleate a second layer at the substrate edges. Increasing the concentration further will nucleate a second layer.

With an excess thiol concentration of 6×10^{-3}, the droplet evaporated under ambient conditions at a rate of ~1 mg min^{-1} until a thin film of dodecanethiol remained[7]. The final stage of drying occurred over several hours. We achieved similar results with lower concentrations of excess thiol by slowing the late-stage drying with a solvent-rich atmosphere. Under both conditions, compact monolayers form that extend over the whole substrate, as shown in Fig. 1.

Growth rates of individual monolayer islands were directly measured using video microscopy. Transmission electron microscopy (TEM) studies on the final product established that we were indeed tracking monolayer islands in the optical microscope. The sample was enclosed to maintain a stable evaporation environment without suppressing evaporation. Neglecting the boundaries, all of the points on the surface of the drop should evaporate at the same rate. As the drop remains pinned at the substrate edges during evaporation, an advection current must transport liquid from the thick region at the centre of the drop to the thin outer perimeter[20]. We estimate for the centre of the drop, that roughly half of the height is lost to evaporation, and the other half to advection. Measurements were made at the centre of the drop where surface flows caused by advection were not observed. For each experiment, a group of islands was tracked, keeping them within the field of view, during the evaporation process. For different time points, island areas were measured for all of the islands that were fully within the frame and in focus. For a given experiment, all of the island growth rates followed the same scaling, as shown in Fig. 3.

Received 16 June 2005; accepted 23 January 2006; published 19 March 2006.

References

1. Deegan, R. D. *et al.* Capillary flow as the cause of ring stains from dried liquid drops. *Nature* **389,** 827–829 (1997).
2. Rabani, E., Reichman, D. R., Geissler, P. L. & Brus, L. E. Drying-mediated self-assembly of nanoparticles. *Nature* **426,** 271–274 (2003).
3. Tang, J., Ge, G. L. & Brus, L. E. Gas-liquid-solid phase transition model for two-dimensional nanocrystal self-assembly on graphite. *J. Phys. Chem. B* **106,** 5653–5658 (2002).
4. Pileni, M. P. Nanocrystal self-assemblies: Fabrication and collective properties. *J. Phys. Chem. B* **105,** 3358–3371 (2001).

5. Wang, Z. L. Structural analysis of self-assembling nanocrystal superlattices. *Adv. Mater.* **10,** 13–30 (1998).
6. Ohara, P. C., Leff, D. V., Heath, J. R. & Gelbart, W. M. Crystallization of opals from polydisperse nanoparticles. *Phys. Rev. Lett.* **75,** 3466–3469 (1995).
7. Lin, X. M., Jaeger, H. M., Sorensen, C. M. & Klabunde, K. J. Formation of long-range-ordered nanocrystal superlattices on silicon nitride substrates. *J. Phys. Chem. B* **105,** 3353–3357 (2001).
8. Narayanan, S., Wang, J. & Lin, X.-M. Dynamical self-assembly of nanocrystal superlattices during colloidal droplet evaporation by in situ small angle X-ray scattering. *Phys. Rev. Lett.* **93,** 135503 (2004).
9. Ge, G. L. & Brus, L. Evidence for spinodal phase separation in two-dimensional nanocrystal self-assembly. *J. Phys. Chem. B* **104,** 9573–9575 (2000).
10. Korgel, B. A. & Fitzmaurice, D. Condensation of ordered nanocrystal thin films. *Phys. Rev. Lett.* **80,** 3531–3534 (1998).
11. Lin, Y., Skaff, H., Emrick, T., Dinsmore, A. D. & Russell, T. P. Nanoparticle assembly and transport at liquid-liquid interfaces. *Science* **299,** 226–229 (2003).
12. Dinsmore, A. D. *et al*. Colloidosomes: Selectively permeable capsules composed of colloidal particles. *Science* **298,** 1006–1009 (2002).
13. Santhanam, V., Liu, J., Agarwal, R. & Andres, R. P. Self-assembly of uniform monolayer arrays of nanoparticles. *Langmuir* **19,** 7881–7887 (2003).
14. Collier, C. P., Vossmeyer, T. & Heath, J. R. Nanocrystal superlattices. *Ann. Rev. Phys. Chem.* **49,** 371–404 (1998).
15. Murray, C. B., Kagan, C. R. & Bawendi, M. G. Self-organization of CdSe nanocrystallites into 3-dimensional quantum-dot superlattices. *Science* **270,** 1335–1338 (1995).
16. Lewis, B. & Campbell, D. S. Nucleation and initial-growth behavior of thin-film deposits. *J. Vac. Sci. Technol.* **4,** 209–218 (1967).
17. Venables, J. A. & Ball, D. J. Nucleation and growth of rare-gas crystals. *Proc. R. Soc. Lond. A* **322,** 331 (1971).
18. Pieranski, P. Two-dimensional interfacial colloidal crystals. *Phys. Rev. Lett.* **45,** 569–572 (1980).
19. Dinsmore, A. D., Warren, P. B., Poon, W. C. K. & Yodh, A. G. Fluid-solid transitions on walls in binary hard-sphere mixtures. *Europhys. Lett.* **40,** 337–342 (1997).
20. Deegan, R. D. *et al*. Contact line deposits in an evaporating drop. *Phys. Rev. E* **62,** 756–765 (2000).

Acknowledgements

We thank M. Constantinides and R. Diamond for their help with early experiments. This work was supported by the UC-ANL Consortium for Nanoscience Research and by the NSF MRSEC program under DMR 0213745. X.-M.L. acknowledges support from the US Department of Energy, Basic Energy Sciences-Materials Sciences, under Contract W-31-109-ENG-38.
Correspondence and requests for materials should be addressed to H M.J.
Supplementary Information accompanies this paper on www.nature.com/naturematerials.

Competing financial interests

The authors declare that they have no competing financial interests.